Journal of Photochemistry & Photobiology, A: Chemistry 461 (2025) 116153

Contents lists available at ScienceDirect

Journal of Photochemistry & Photobiology, A: Chemistry

journal homepage: www.elsevier.com/locate/jphotochem

On the valence shell spectroscopy of 1,2-dichlorobenzene

L.V.S. Dalagnol [a,1], S. Kumar [b,c,2], A.Souza Barbosa [a,3], U.S. Akther [b], N.C. Jones [d,4], S.V. Hoffmann [d,5], M.H.F. Bettega [a,6,*], P. Limão-Vieira [a,b,7,*]

[a] Departamento de Física, Universidade Federal do Paraná, Caixa Postal 19044, 81531-980 Curitiba, Paraná, Brazil
[b] Atomic and Molecular Collisions Laboratory, CEFITEC, Department of Physics, NOVA School of Science and Technology, Universidade NOVA de Lisboa, 2829-516 Caparica, Portugal
[c] Chemical Sciences Division, Lawrence Berkeley National Laboratory, One Cyclotron Road, Berkeley 94720, CA, USA
[d] ISA, Department of Physics and Astronomy, Aarhus University, Ny Munkegade 120, DK-8000 Aarhus C, Denmark

ARTICLE INFO

Keywords:
1,2-dichlorobenzene
Cross-sections
Theoretical calculations
Spectroscopy

ABSTRACT

We report high-resolution vacuum ultraviolet (VUV) photoabsorption spectrum of 1,2-dichlorobenzene in the photon energy range 4.0–10.8 eV (310–115 nm). The electronic state spectroscopy of *ortho*-$C_6H_4Cl_2$ has been investigated together with quantum chemical calculations at different levels of theory, also providing vertical excitation energies and oscillator strengths. The valence, mixed valence-Rydberg and Rydberg character of the electronic transitions is accompanied by fine structure which has been mainly assigned to in-plane breathing with C–Cl stretching, $\nu'_7(a_1)$, ring breathing and C–C stretching, $\nu'_8(a_1)$, in-plane ring breathing, $\nu'_9(a_1)$, C–Cl symmetric stretching, $\nu'_{10}(a_1)$, and in-plane C–Cl bending $\nu'_{11}(a_1)$ modes. The experimental absolute photoabsorption cross sections have been used to calculate the photolysis lifetime of 1,2-dichlorobenzene in the Earth's atmosphere (0–50 km), showing that solar photolysis is expected to be a weak sink at altitudes lower than 20 km relative to •OH radical reactions. Potential energy curves for the lowest-lying excited electronic states, as a function of the C–Cl stretching and in-plane C–Cl bending coordinates, were also obtained employing the time dependent density functional theory (TD-DFT) method. The results show the importance of the complex quasi-degenerate nature of the lowest-lying electronic states which in the intricate nuclear dynamics of the reaction coordinates, yield relevant internal conversion from Rydberg to valence character and in the asymptotic limit bond excision.

1. Introduction

Over the last decade, we have been conducting a thorough investigation into the electronic state spectroscopy of different polyatomic molecules due to their relevance in different industrial, technological, atmospheric, interstellar medium and even biological applications [1] (and references therein), just to mention a few. The knowledge gained from the combined experimental and theoretical methodologies employed, *viz.* high-resolution vacuum ultraviolet (VUV) photoabsorption measurements with state-of-the-art quantum chemical calculations at different levels of theory, have allowed the assignment of neutral lowest-lying electronic excitations that may lead to bond excision with neutral radical formation, see e.g. [2–7]. Moreover, such studies shed light on the underlying molecular mechanisms responsible for relevant internal conversion, e.g. from Rydberg to valence, that govern the rather complex nuclear dynamics within the multidimensional molecular landscape. The most recent cases are formic acid [8] and 2-chlorotoluene [9] molecules.

* Corresponding authors.
E-mail addresses: bettega@fisica.ufpr.br (M.H.F. Bettega), plimaovieira@fct.unl.pt (P. Limão-Vieira).
[1] 0000-0002-5203-3774.
[2] 0000-0002-1996-9925.
[3] 0000-0001-7989-1878.
[4] 0000-0002-4081-6405.
[5] 0000-0002-8018-5433.
[6] 0000-0001-9322-1360.
[7] 0000-0003-2696-1152.

https://doi.org/10.1016/j.jphotochem.2024.116153
Received 4 October 2024; Received in revised form 5 November 2024; Accepted 9 November 2024
Available online 15 November 2024

Chlorobenzene and its derivatives are of interest to the international scientific community for their wide application as precursors to other compounds used in chemical and pharmaceutical industries [10–12]. Such halogenated chemical compounds are also known to be potentially toxic when disposed of in the environment, contributing to soil, groundwater and surface water contaminations [13,14], despite being toxic to human beings. 1,2-dichlorobenzene or *ortho*-dichlorobenzene (*o*-$C_6H_4Cl_2$) is a special case of a molecular compound used as a solvent in organic photovoltaic devices for large-scale commercial use [14,15], also posing a relevant concern as to its environmental impact [14–16]. A literature survey shows no detailed description of the electronic states of 1,2-dichlorobenzene in the ultraviolet photon energy region, as in the present study. Therefore, this information is needed for a description of the molecular structure, but more relevant to assign the nature of the lowest-lying electronic states. The 1,2-dichlorobenzene molecule has been investigated by gas-phase VUV absorption in the energy range from 43 000 to 60 000 cm^{-1} (5.331 to 7.439 eV) [17], infrared and Raman spectroscopy [18] and rate constants for its reactions with •OH radicals [13]. The lowest-lying ionisation energies have been reported by He(I) photoelectron spectroscopy [19–21], photoionisation [22], Penning ionisation electron spectroscopy [23] and charge-transfer equilibrium constant measurements [24]. Also relevant to the present work, is mass-analysed threshold ionisation spectroscopy reporting vibrationally resolved spectra of the first electronically excited state and the cation ground-state [16]. We note the recent experimental and theoretical work on the geometrical effect of *ortho* positions in C_6Cl_6 and 1,2-$C_6H_4Cl_2$ yielding Cl_2^- without any energy constraints from electron transfer experiments, while Cl_2 formation was reported to proceed in the neutral system through a < 2.0 eV energy barrier [25].

The present work combines novel experimental and theoretical methods on the nature of the electronic states of 1,2-dichlorobenzene. High-resolution VUV radiation in the photon energy range from 4.0 to 10.8 eV has been provided from a synchrotron light source to obtain absolute photoabsorption cross-sections, while time-dependent density functional theory (TD-DFT/CAMB3LYP/aug-cc-pVDZ) calculations provide energies and oscillator strengths for the lowest-lying neutral states. The experimental absolute cross-section values have been used to estimate the molecule's lifetime in the Earth's atmosphere (from 0 up to 50 km altitude). Finally, potential energy curves were obtained for the ten lowest-lying excited singlet states, plotted following the C–Cl stretching and in-plane C–Cl bending modes, while allowing all other bond lengths and angles to relax according to the respective mode.

2. Experimental method

The high-resolution VUV photoabsorption spectrum of 1,2-dichlorobenzene in the energy range from 4.0 eV to 10.8 eV (Figs. 1–5) was measured at the AU-UV beam line of the ASTRID2 synchrotron facility at Aarhus University, Denmark. The experiments were performed in an absorption gas cell end station, which has been described before [26,27]. Briefly, synchrotron radiation passes through a static gas sample filled with 1,2-dichlorobenzene vapour at room temperature with the transmitted light detected by a photomultiplier tube (PMT). At both ends of the absorption cell, MgF_2 transmission windows define the low wavelength detection limit to 115 nm. The gas sample number density in the absorption cell is obtained by recording the absolute pressure of 1,2-dichlorobenzene measured by a capacitance manometer (Chell CDG100D), while the absorption cross-sections were measured in the pressure range 0.02–1.32 mbar, to achieve attenuations of 50 % or less and hence avoiding saturation effects.

The Beer-Lambert attenuation law, $I_t = I_0 e^{(-N\sigma l)}$, was used to obtain the absolute photoabsorption cross-sections values, σ, in units of megabarn (1 Mb $\equiv 10^{-18}$ cm^2), where I_t is the light intensity transmitted through the gas sample, I_0 is that through the evacuated cell, N the molecular number density of 1,2-dichlorobenzene, and l the absorption path length (15.5 cm). Throughout the collection of each spectrum, the synchrotron beam current was monitored, and background scans, I_0, were recorded with the cell evacuated. Within the wavelength region scanned (115–310 nm), accurate cross-section values are obtained by recording the VUV spectrum in small (5 or 10 nm) sections, allowing an overlap of at least 10 points between the adjoining sections. ASTRID2 operates in a "top-up" mode allowing the light intensity to be kept quasi-constant, thus compensating for the constant beam decay in the storage ring. The variations (2–3 %) of the incident flux are therefore normalized to the beam current in the storage ring. This methodology allows us to determine photoabsorption cross-sections to an accuracy of ± 5 %. The resolution in the present spectrum is better than 0.08 nm [26], which corresponds to 1, 3, and 7 meV at the low extreme, the midpoint, and the high extreme of the photon energy range scanned, respectively.

The liquid sample used in the VUV photoabsorption measurements

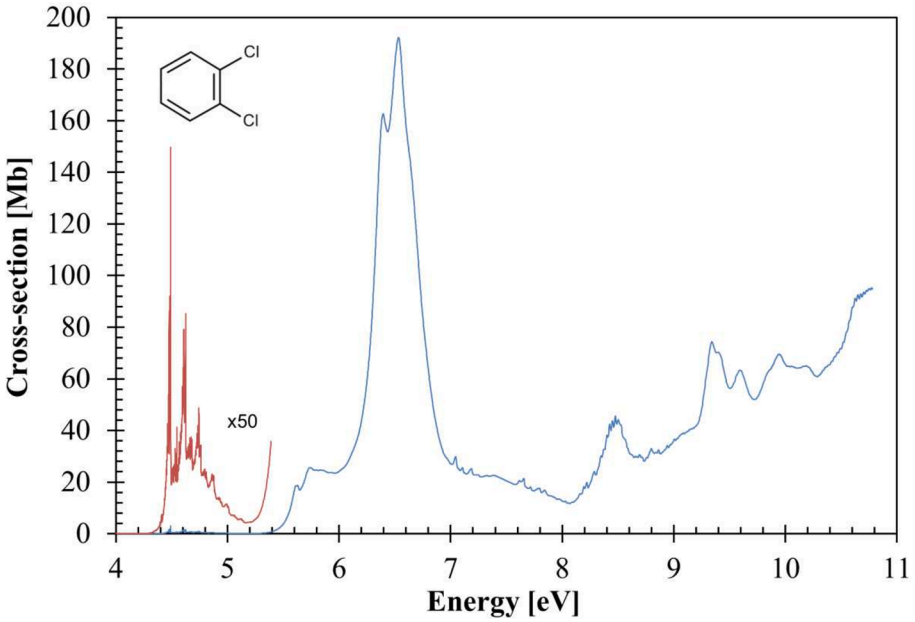

Fig. 1. The high-resolution photoabsorption spectrum of 1,2-dichlorobenzene in the 4.0–10.8 eV photon energy range. See text for details.

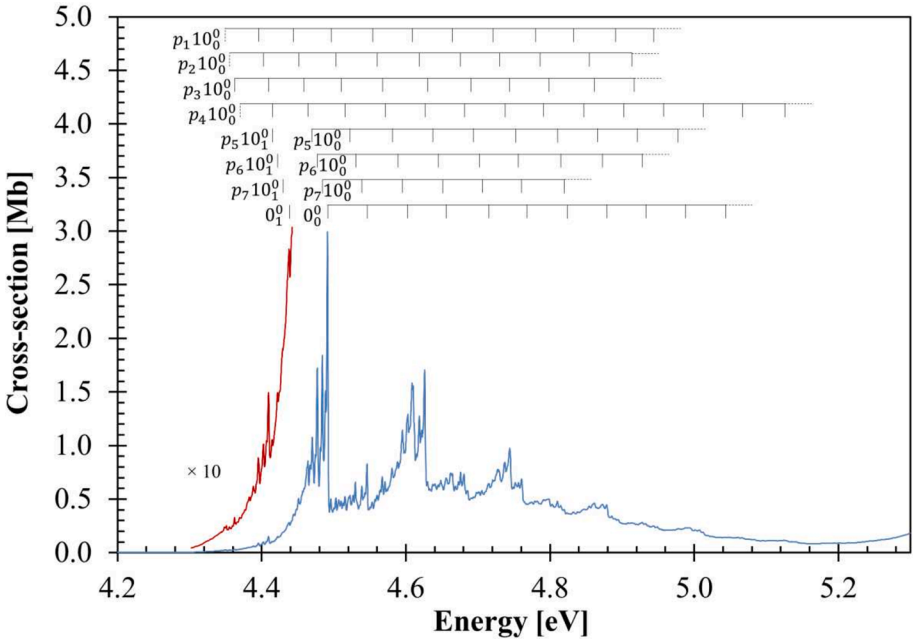

Fig. 2. Detail of the photoabsorption spectrum of 1,2-dichlorobenzene in the 4.2–5.3 eV photon energy. See text for details.

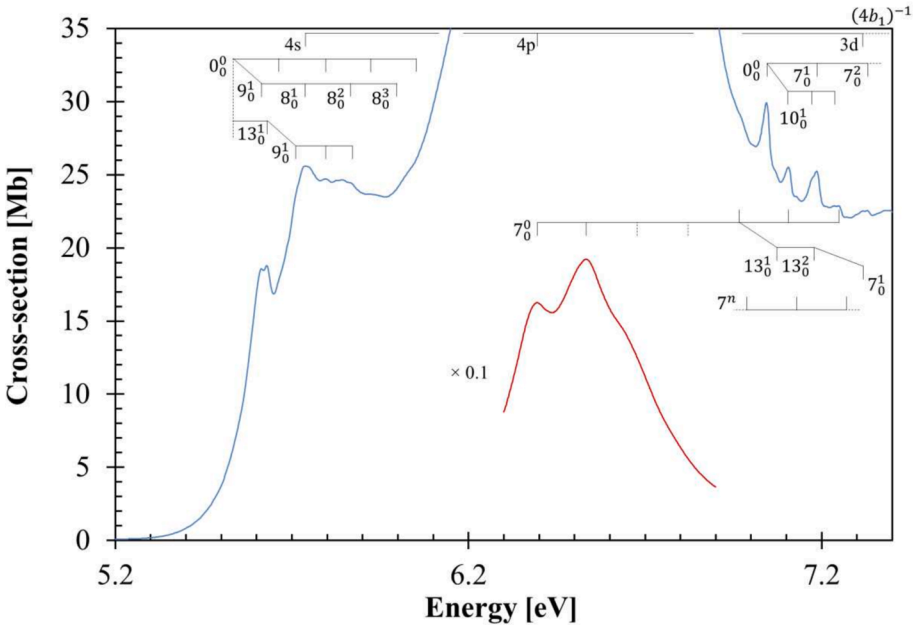

Fig. 3. Detail of the photoabsorption spectrum of 1,2-dichlorobenzene in the 5.2–7.4 eV photon energy range with Rydberg series converging to $(4b_1)^{-1}\ \widetilde{X}^2B_1$. See text for details.

was purchased from Sigma-Aldrich, with a stated purity of ≥ 98 %. The sample was degassed through repeated freeze–pump–thaw cycles before use.

3. Theoretical methods

The identification of the major electronically excited states of 1,2-dichlorobenzene has been performed with the help of quantum chemical calculations at different levels of theory. The molecular and electronic structures obtained have been crucial to assign the different features in the photoabsorption spectrum. The vertical excitation energies and oscillator strengths of the most important electronically excited states in Table 1 (see also Supporting Material Table S1), were calculated employing TD-DFT [28,29] with a CAMB3LYP functional [30], and the aug-cc-pVDZ basis set [31] as implemented in GAMESS-US computational package [32]. The nature of each excitation was assessed by visual inspection of the natural orbitals for each transition. The calculated vertical excitation energy of the lowest-lying excited state at 5.180 eV, is 11 % higher than the experimental value, thus we have performed additional calculations to check if a better agreement could be attained. The results from the equation of motion coupled-cluster with singles and doubles excitations (EOM-CCSD) [33–36], with the aug-cc-pVDZ basis set as implemented in GAMESS-US [32] are shown in Table S2. Harmonic frequencies (CAMB3LYP/aug-cc-pVDZ) for the

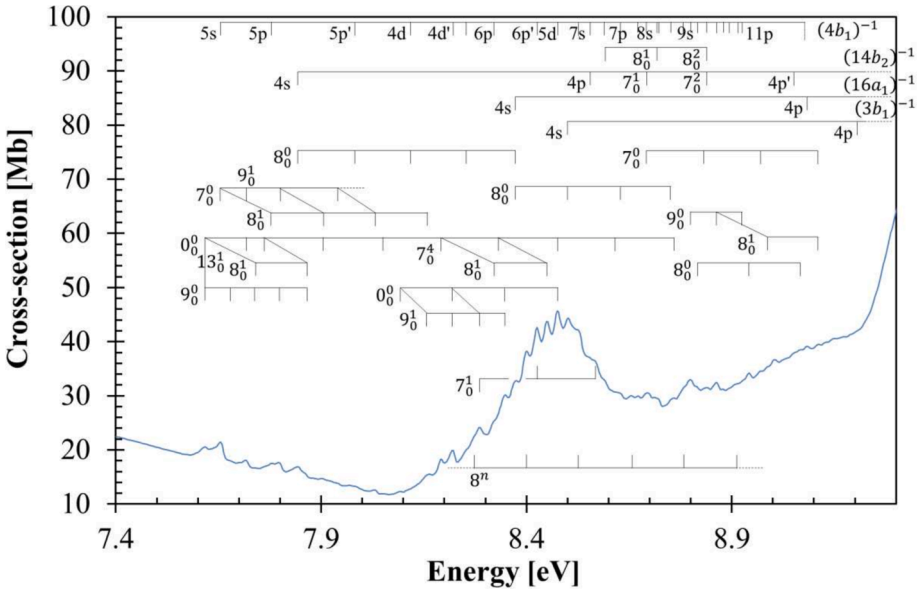

Fig. 4. Detail of the photoabsorption spectrum of 1,2-dichlorobenzene in the 7.4–9.3 eV photon energy range with Rydberg series converging to $(4b_1)^{-1}$ $\widetilde{X}^2B_1$, $(14b_2)^{-1}$ $\widetilde{B}^2B_2$, $(16a_1)^{-1}$ $\widetilde{C}^2A_1$ and $(3b_1)^{-1}$ $\widetilde{D}^2B_1$. See text for details.

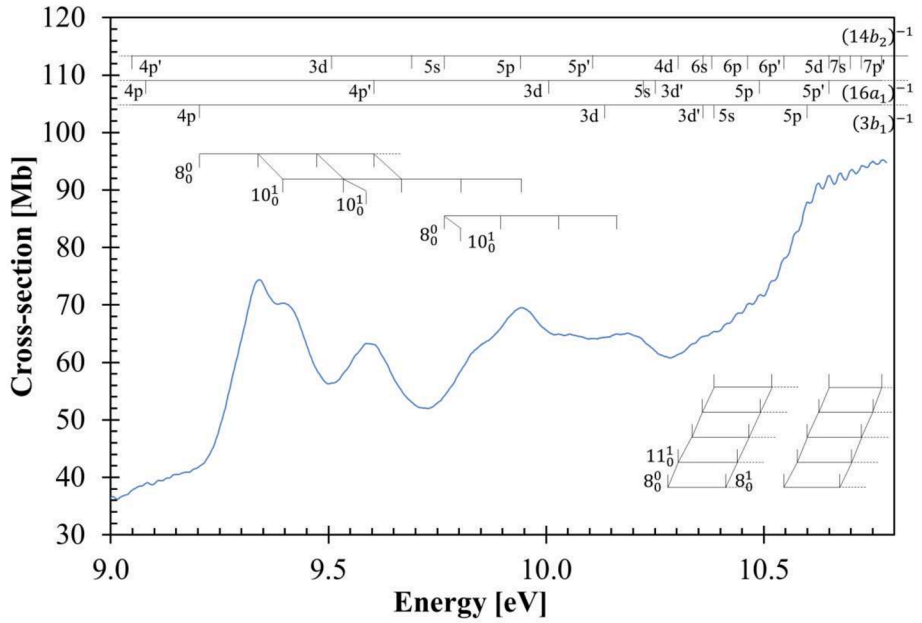

Fig. 5. Detail of the photoabsorption spectrum of 1,2-dichlorobenzene in the 9.0–10.8 eV photon energy range with Rydberg series converging to $(14b_2)^{-1}$ $\widetilde{B}^2B_2$, $(16a_1)^{-1}$ $\widetilde{C}^2A_1$ and $(3b_1)^{-1}$ $\widetilde{D}^2B_1$. See text for details.

neutral electronic ground-state (Table S3), the neutral electronic first excited-state (Table S4) and the cationic electronic ground-state (Table S5) have also been obtained.

4. Structure and properties of 1,2-dichlorobenzene

The neutral ground-state, neutral first excited-state and cationic ground-state geometries of 1,2-dichlorobenzene obtained at the DFT/CAMB3LYP/aug-cc-pVDZ level, together with their bond lengths (Å) and bond angles (°) are listed in the Supporting Material (Figs. S1–S3). The calculated outermost electronic configuration of the $\widetilde{X}^1A_1$ ground-state (Fig. S1) is … $(2b_1)^2$ $(13b_2)^2$ $(15a_1)^2$ $(2a_2)^2$ $(3b_1)^2$ $(16a_1)^2$ $(14b_2)^2$ $(3a_2)^2$ $(4b_1)^2$. The ground-state MOs character displayed in Fig. S4 show the highest occupied molecular orbital (HOMO), $4b_1$, is the Cl 3p lone pair orbital (n_{Cl}) out-of-plane with ring π(C = C) character. The second highest occupied molecular orbital (HOMO-1), $3a_2$, is (n_{Cl}) and π(C = C), the (HOMO-2), $14b_2$, and (HOMO-3), $16a_1$, are ($\overline{n}_{Cl}$) in the molecular plane with σ_{CC} character. Other MOs from which electrons can be excited (HOMO-4), $3b_1$, and (HOMO-5), $2a_2$, are (n_{Cl}) and ($\overline{n}_{Cl}$), also both with π(C = C) character, while (HOMO-6), $15a_1$, and (HOMO-8), $2b_1$, are σ_{CCl}/σ_{CC} and $\overline{n}_{Cl}/\pi$ bonding in character. The major absorption features in Figs. 1–5 are due to electronic excitations from these MOs to valence, mixed valence-Rydberg and Rydberg orbitals, with the calculated dominant excitation energies and oscillator strengths listed in Table 1 (for the complete set of calculated electronic transitions see Table S1).

Table 1
The most representative calculated vertical excitation energies (TD-DFT/CAMB3LYP/aug-cc-pVDZ) and oscillator strengths of 1,2-dichlorobenzene compared with the present experimental data. Energies in eV. See text for details.

1,2-dichlorobenzene				E (eV) expt.[a]	Cross-section (Mb)
State	E (eV)	f_L	Dominant excitations		
$\widetilde{X}\ ^1A_1$					
$2\ ^1A_1$	5.180	0.0050	$\pi^*(5b_1) \leftarrow n_{Cl}/\pi(4b_1)$ (63 %) + $\pi^*(4a_2) \leftarrow n_{Cl}/\pi(3a_2)$ (35 %)	4.626	1.7
$1\ ^1B_2$	5.784	0.0405	$\pi^*(4a_2) \leftarrow n_{Cl}/\pi(4b_1)$ (65 %) + $\pi^*(5b_1) \leftarrow n_{Cl}/\pi(3a_2)$ (33 %)	5.740	25.59
$3\ ^1A_1$	6.521	0.6503	$\pi^*(4a_2) \leftarrow n_{Cl}/\pi(3a_2)$ (61 %) + $\pi^*(5b_1) \leftarrow n_{Cl}/\pi(4b_1)$ (35 %)	6.536	192.01
$2\ ^1B_1$	6.525	0.0238	$4s/\sigma^*_{CCl}(17a_1) \leftarrow n_{Cl}/\pi(4b_1)$ (57 %) + $4s/\sigma^*_{CCl}(18a_1) \leftarrow n_{Cl}/\pi(4b_1)$ (30 %)		
$4\ ^1A_1$	7.892	0.0204	$4p/\pi^*(6b_1) \leftarrow n_{Cl}/\pi(4b_1)$ (54 %) + $\sigma^*_{CCl}/\sigma^*_{CH}(19a_1) \leftarrow \overline{n}_{Cl}/\sigma_{CC}(16a_1)$ (13 %)	7.185	25.25
$6\ ^1A_1$	8.371	0.0815	$\pi^*(5b_1) \leftarrow n_{Cl}/\pi(3b_1)$ (63 %)	7.656	21.44
$6\ ^1B_2$	8.627	0.0951	$5d/\pi^*(5a_2) \leftarrow n_{Cl}/\pi(4b_1)$ (58 %) + $\pi^*(5b_1) \leftarrow \overline{n}_{Cl}/\pi(2a_2)$ (28 %)	8.475	45.64
$10\ ^1B_2$	9.453	0.0829	$4p(15b_2) \leftarrow \overline{n}_{Cl}/\sigma_{CC}(16a_1)$ (33 %) + $3d/\sigma^*_{CCl}(20a_1) \leftarrow \overline{n}_{Cl}/\sigma_{CC}(14b_2)$ (15 %) + $\sigma^*_{CCl}/\sigma^*_{CH}(19a_1) \leftarrow \overline{n}_{Cl}/\sigma_{CC}(14b_2)$ (11 %) + $3d(16b_2) \leftarrow \overline{n}_{Cl}/\sigma_{CC}(16a_1)$ (11 %) + $6d/\pi^*(6a_2) \leftarrow n_{Cl}/\pi(4b_1)$ (11 %)	9.167	40.52
$21\ ^1B_1$	9.994	0.0557	$6s/\sigma^*_{CCl}(18a_1) \leftarrow n_{Cl}/\pi(4b_1)$ (20 %) + $\sigma^*_{CCl}/\sigma^*_{CH}(19a_1) \leftarrow n_{Cl}/\pi(4b_1)$ (18 %) + $6d/\sigma^*_{CCl}(19b_2) \leftarrow n_{Cl}/\pi(3a_2)$ (11 %)	9.343	74.32
$16\ ^1B_2$	10.357	0.0742	$4d/\pi^*(9b_1) \leftarrow n_{Cl}/\pi(3a_2)$ (41 %) + $4d/\pi^*(10b_1) \leftarrow n_{Cl}/\pi(3a_2)$ (12 %)	9.94(1)	69.49
$21\ ^1A_1$	10.463	0.0553	$3d(21a_1) \leftarrow \overline{n}_{Cl}/\sigma_{CC}(16a_1)$ (25 %) + $5s/\sigma^*_{CCl}(18a_1) \leftarrow \sigma_{CCl}/\sigma_{CC}(15a_1)$ (23 %) + $\sigma^*_{CCl}/\sigma^*_{CH}(19a_1) \leftarrow \sigma_{CCl}/\sigma_{CC}(15a_1)$ (16 %)		
$22\ ^1A_1$	10.505	0.0554	$\pi^*(5b_1) \leftarrow \overline{n}_{Cl}/\pi(2b_1)$ (81 %)		

[a] the last decimal of the energy value is given in brackets for these less-resolved features;

The expanded views of the measured cross-sections in Figs. 2–5 show fine structure which has been assigned to vibronic transitions, with main vibrational modes assigned according to the experimental photoelectron spectrum of Holland *et al.* [19] and Raman and infrared spectroscopies of Green [18]. Additional information has been obtained from the calculation of the harmonic frequencies and labelling in Tables S3–S5. The main modes have been assigned based on the energies (and wavenumbers) in the neutral electronic ground-state to 0.140 eV (1130 cm^{-1}) for in-plane breathing with C–Cl stretching, $\nu''_7(a_1)$, 0.129 eV (1040 cm^{-1}) for ring breathing and C–C stretching, $\nu''_8(a_1)$, 0.082 eV (660 cm^{-1}) in-plane ring breathing, $\nu''_9(a_1)$, 0.060 eV (480 cm^{-1}) C–Cl symmetric stretching, $\nu''_{10}(a_1)$, 0.025 eV (203 cm^{-1}) for in-plane C–Cl bending $\nu''_{11}(a_1)$ and 0.105 eV (850 cm^{-1}) for C–H wagging $\nu''_{13}(a_2)$. Note that neutral electronic first excited-state harmonic frequencies from Table S4 have been also considered in the assignment of the fine structure. Moreover, for the Rydberg character of the electronic transitions, the main vibrational modes have been assigned from the experimental photoelectron spectroscopy data [19] to 0.136 eV (1097 cm^{-1}) for in-plane breathing with C–Cl stretching, $\nu'_7(a_1)$, 0.126 eV (1016 cm^{-1}) for ring breathing and C–C stretching, $\nu'_8(a_1)$, 0.079 eV (637 cm^{-1}) in-plane ring breathing, $\nu'_9(a_1)$, 0.059 eV (476 cm^{-1}) C–Cl symmetric stretching, $\nu'_{10}(a_1)$ and 0.026 eV (210 cm^{-1}) for in-plane C–Cl bending $\nu'_{11}(a_1)$ (see Sec. 5.2).

For the assignment of fine structure, we adopt the notation X^n_m, with m and n denoting the initial and final vibrational states for the vibronic structure (X). Of relevance is that more than one mode may contribute to the absorption features, implying that the normal mode description of vibrations is very powerful for the lowest lying excitations, with the possibility of Fermi resonances. The tentative assignment of the different Rydberg orbitals has been performed based on the quantum defects and the ionisation energies (IEs) from the photoelectron data of Holland and co-workers [19] to be $IE_1 = 9.075\ (4b_1)^{-1}$, $IE_3 = 11.239\ (14b_2)^{-1}$, $IE_4 = 11.769\ (16a_1)^{-1}$ and $IE_5 = 11.897$ eV $(3b_1)^{-1}$. The MO numbering from which an electron is removed, is different from Holland's Hartree-Fock electronic configuration, however with the same character as in the present calculations. Also note that no attempt was made to assign Rydberg series converging to $(3a_2)^{-1}$ ($IE_2 = 9.643$ eV) and $(2a_2)^{-1}$ ($IE_6 = 12.372$ eV) because the electronic transitions are dipole forbidden within the molecule's C_{2v} group symmetry.

5. Results and discussion

The complete photoabsorption spectrum of 1,2-dichlorobenzene in the energy range 4.0 to 10.8 eV is shown in Fig. 1, with enlarged sections in Figs. 2–5. The assignments of the different absorption features listed in Tables 1–6 contain the major electronic excitations (and also vibrational excitations) from the ground-state to valence, mixed valence-Rydberg and Rydberg character molecular orbitals converging to the $(4b_1)^{-1}\ \widetilde{X}^2B_1$, $(14b_2)^{-1}\ \widetilde{B}^2B_2$, $(16a_1)^{-1}\ \widetilde{C}^2A_1$ and $(3b_1)^{-1}\ \widetilde{D}^2B_1$ ionic electronic states (see Sec. 5.4). All absorption bands exhibit extensive fine structure in particular for the lowest-lying electronic state in the photon energy range 4.2–5.3 eV (Fig. 2). In this region, the progressions have been assigned to the C–Cl symmetric stretching, $\nu'_{10}(a_1)$ mode, while from 5.2 up to 10.8 eV (Figs. 3–5) the dominant modes are in-plane breathing with C–Cl stretching, $\nu'_7(a_1)$, ring breathing and C–C stretching, $\nu'_8(a_1)$, in-plane ring breathing, $\nu'_9(a_1)$, C–Cl symmetric stretching, $\nu'_{10}(a_1)$ and in-plane C–Cl bending $\nu'_{11}(a_1)$. Throughout the spectrum, except for the lowest-lying band (4.2–5.3 eV) of valence character, the photoabsorption features result from the contribution of several overlapping mixed valence-Rydberg and Rydberg transitions accompanied by vibrational excitation. The overall effect is reflected in some sections displaying broader absorption features. The TD-DFT calculated vertical excitation energies are shown in Table 1 and are compared with the experimental data. A reasonably good level of agreement (to within ± 9 %) is noted apart from the $\left(2^1A_1 \leftarrow \widetilde{X}^1A_1\right)$ transition. Additional calculations at a different level of theory were performed with EOM-CCSD/aug-cc-pVDZ (Table S2), with the molecular orbitals' electron densities in Fig. S5. The relevant difference pertains only to the lowest-lying absorption band at 4.854 eV which shows a better agreement (< 5 %) with the experimental value at 4.626 eV. The assignments of the vibrational modes contributing to the spectrum for each electronic transition are detailed in Tables 2–5.

5.1. The 4.2–5.3 eV photon energy range

The lowest-lying valence transition is assigned to the promotion of the chlorine lone pair out-of-plane (n_{Cl}) with ring π(C = C) MO to the π* (4a_2) and π*(5b_1) antibonding orbitals, $\pi^*(5b_1) \leftarrow n_{Cl}/\pi(4b_1) + \pi^*(4a_2) \leftarrow n_{Cl}/\pi(3a_2)$, $\left(2^1A_1 \leftarrow \widetilde{X}^1A_1\right)$. The vertical excitation energy value of 4.626 eV, with a cross-section of 1.7 Mb, is in good agreement with the EOM-CCSD calculated value of 4.854 eV (Table S2). The oscillator strength

Table 2
Proposed vibrational assignments of 1,2-dichlorobenzene valence and Rydberg series converging to the different ionic states in the photon energy range 4.2 – 5.3 eV[a]. Energies in eV. See text for details.

This work		
assignment	energy	ΔE (ν'_{10})
$\pi^*(5b_1)\leftarrow n_{Cl}/\pi(4b_1) + \pi^*(4a_2)\leftarrow n_{Cl}/\pi(3a_2), \left(2^1A_1\leftarrow\tilde{X}^1A_1\right)$		
$p_1 10_0^0$	4.34(7)(b,w)	0.0 (−0.144)
$p_2 10_0^0$	4.35(4)(b,w)	0.0 (−0.137)
$p_3 10_0^0$	4.362	0.0 (−0.129)
$p_4 10_0^0$	4.37(3)(b,w)	0.0 (−0.118)
$p_1 10_0^1$	4.396	0.049
$p_2 10_0^1$	4.402	0.048
$p_3 10_0^1$	4.410	0.048
$p_5 10_1^0/p_4 10_0^1$	4.417	– / 0.044
$p_6 10_1^0$	4.425	–
$p_7 10_1^0$	4.43(0)(s)	–
0_1^0	4.438	–
$p_1 10_0^2$	4.445	0.049
$p_2 10_0^2$	4.451	0.049
$p_3 10_0^2$	4.46(0)(s)	0.050
$p_4 10_0^2$	4.464	0.047
$p_5 10_0^0$	4.470	0.0 (−0.021)
$p_6 10_0^0$	4.477	0.0 (−0.014)
$p_7 10_0^0$	4.484	0.0 (−0.007)
0_0^0	4.491	0.0
$p_1 10_0^3$	4.496	0.051
$p_2 10_0^3$	4.503	0.052
$p_3 10_0^3$	4.51(1)(w)	0.051
$p_4 10_0^3$	4.516	0.052
$p_5 10_0^1$	4.523	0.053
$p_6 10_0^1$	4.530	0.053
$p_7 10_0^1$	4.539	0.055
10_0^1	4.546	0.055
$p_1 10_0^4$	4.554	0.058
$p_2 10_0^4$	4.560	0.057
$p_3 10_0^4$	4.567	0.056
$p_4 10_0^4$	4.571	0.055
$p_5 10_0^2$	4.581	0.058
$p_6 10_0^2$	4.589	0.059
$p_7 10_0^2$	4.595	0.056
10_0^2	4.603	0.057
$p_1 10_0^5$	4.609	0.055
$p_2 10_0^5$	4.619	0.059
$p_3 10_0^5$	4.63(0)(s)	0.063
$p_4 10_0^5$	4.626	0.055
$p_5 10_0^3$	4.63(8)(w)	0.057
$p_6 10_0^3$	4.64(7)(s)	0.058
$p_7 10_0^3$	4.65(4)(s,w)	0.059
10_0^3	4.657	0.054
$p_1 10_0^6$	4.66(5)(s)	0.056
$p_2 10_0^6$	4.679	0.057
$p_3 10_0^6$	4.69(2)(w)	0.062
$p_4 10_0^6$	4.681	0.055
$p_5 10_0^4$	4.69(6)(s,w)	0.058
$p_6 10_0^4$	4.702	0.055
$p_7 10_0^4$	4.706	0.052
10_0^4	4.716	0.059
$p_1 10_0^7$	4.72(3)(w)	0.058
$p_2 10_0^7$	4.72(9)(s)	0.053
$p_4 10_0^7$	4.737	0.056
$p_3 10_0^7$	4.744	0.052
$p_5 10_0^5$	4.752	0.056
$p_6 10_0^5$	4.757	0.055
$p_7 10_0^5$	4.761	0.055
10_0^5	4.77(1)(s,w)	0.055
$p_1 10_0^8$	4.78(2)(w)	0.059
$p_2 10_0^8$	4.78(9)(s,w)	0.060
$p_4 10_0^8$	4.79(3)(b,w)	0.056
$p_3 10_0^8$	4.79(9)(b)	0.055
$p_5 10_0^6$	4.810	0.058
$p_6 10_0^7$	4.815	0.058
$p_7 10_0^6$	4.82(0)(s,w)	0.059
10_0^6	4.82(6)(s,w)	0.055
$p_1 10_0^9$	4.83(4)(w)	0.052
$p_4 10_0^9$	4.85(0)(b,w)	0.057
$p_2 10_0^9$	4.85(5)(w)	0.066
$p_5 10_0^7$	4.85(8)(s,w)	0.058
$p_3 10_0^9$	4.86(2)(b)	0.063
$p_6 10_0^7$	4.873	0.058
10_0^7	4.879	0.053
$p_1 10_0^{10}$	4.89(1)(s)	0.057
$p_4 10_0^{10}$	4.90(4)(b,w)	0.054
$p_2 10_0^{10}$	4.91(5)(b,w)	0.060
$p_3 10_0^{10}$	4.91(8)(b,w)	0.056
$p_5 10_0^8$	4.92(3)(s,w)	0.055
$p_6 10_0^8$	4.92(9)(b,w)	0.056
10_0^8	4.93(4)(s,w)	0.055
$p_1 10_0^{11}$	4.94(5)(w)	0.054
$p_4 10_0^{11}$	4.95(9)(w)	0.055
$p_5 10_0^9$	4.98(0)(s,w)	0.057
10_0^9	4.99(0)(b,w)	0.056
$p_4 10_0^{12}$	5.01(4)(s)	0.055
10_0^{10}	5.04(6)(w)	0.056
$p_4 10_0^{13}$	5.06(9)(w)	0.055
$p_4 10_0^{14}$	5.12(8)(b,w)	0.059
	$\overline{\Delta E}$	0.055

[a] (b) broad feature; (w) weak feature; (s) shoulder structure (the last decimal of the energy value is given in brackets for these less-resolved features).

obtained at the TD-DFT level of theory (see Table 1) is 25 % lower than the EOM-CCSD result, however with a poor agreement of the calculated energy relative to the experimental data.

Fig. 2 shows in detail the fine structure due to vibronic excitation in the 4.2–5.3 eV energy region. The 0_0^0 origin of the band at 4.490 eV has been reported by Gaber *et al.* [16] from (1 + 1′) resonance-enhanced multiphoton ionisation experiments, in excellent agreement with the present work at 4.491 eV. This band shows many progressions that are listed in Table 2 and have been assigned to the contribution of several 10_0^n ($n = 1$–14) progressions from the C–Cl symmetric stretching, $\nu'_{10}(a_1)$ mode, with an average spacing of 0.055 eV (∼ 444 cm^{-1}). Such assignment is in agreement with the first excited state mass analysed threshold ionisation spectroscopy of 1,2-dichlorobenzene, while other vibrational modes can also be active [16,37]. Thus, we do not discard the possibility of additional assignments, in particular the in-plane breathing with C–Cl stretching, $\nu'_7(a_1)$ mode.

The geometries of 1,2-dichlorobenzene in the ground-state and first excited-state, together with their bond lengths in Å and bond angles in (°), are shown in Fig. S1 and S2. Upon electronic excitation, a small increase in the C–C bond lengths (∼ 2 %) and in the Cl/Cl interatomic distance are noted, the latter from the modest reduction in the Cl7–C1–C6 and C2–C3–Cl8 angles (< 1 %) between the neutral ground-state and the first excited-state. Another interesting aspect is related to the change in the C1–Cl7 and C2–Cl8 bond lengths from 1.732 Å in the ground-state to 1.705 Å in the first excited-state (Figs. S1 and S2). Such changes are in agreement with C–Cl symmetric stretching $\nu'_{10}(a_1)$ mode assigned in Fig. 2, whereas C–C bond lengthening may also render contributions from in-plane breathing with C–Cl stretching, $\nu'_7(a_1)$ mode.

Table 3
Proposed vibrational assignments of 1,2-dichlorobenzene valence and Rydberg series converging to the different ionic states in the photon energy range 5.2 – 7.4 eV[a]. Energies in eV. See text for details.

assignment	energy	ΔE (ν'_7)	ΔE (ν'_8)	ΔE (ν'_9)	ΔE (ν'_{10})	ΔE (ν'_{13})
$\pi^*(4a_2)\leftarrow n_{Cl}/\pi(4b_1) + \pi^*(5b_1)\leftarrow n_{Cl}/\pi(3a_2), \left(1^1B_2\leftarrow\widetilde{X}^1A_1\right)$						
0_0^0	5.53(5) (s,w)	–	–	–	–	–
9_0^1	5.613	–	–	0.078	–	–
13_0^1	5.628	–	–	–	–	0.093
8_0^1	5.66(7) (s)	–	0.132	–	–	–
$13_0^1 9_0^1$	5.71(1) (s)	–		0.083	–	–
$9_0^1 8_0^1/4s(4b_1)^{-1}$	5.73(5) (b)	–	0.122	0.068	–	–
$8_0^2/13_0^1 9_0^2$	5.79(6) (b)	–	0.129	0.061/ 0.069	–	–
$9_0^1 8_0^2/13_0^1 9_0^3$	5.86(5) (b)	–	0.130	0.069/ 0.085	–	–
8_0^3	5.92(8) (b,w)	–	0.132	0.063	–	–
$9_0^1 8_0^3$	6.00(0) (s,w)	–	0.135	0.072	–	–
8_0^4	6.05(5) (s,w)	–	0.127	0.055	–	–
$\pi^*(4a_2)\leftarrow n_{Cl}/\pi(3a_2) + \pi^*(5b_1)\leftarrow n_{Cl}/\pi(4b_1), \left(3^1A_1\leftarrow\widetilde{X}^1A_1\right)$						
$4p(4b_1)^{-1}$	6.394	–	–	–	–	–
7_0^1	6.532	0.138	–	–	–	–
7_0^2	6.67(8) (s,w)	0.146	–	–	–	–
7_0^3	6.82(4) (s,w)	0.146	–	–	–	–
7_0^4	6.96(5) (s)	0.141	–	–	–	–
$7_0^4 13_0^1$	7.07(1) (s)	–	–	–	–	0.106
7_0^5	7.107	0.142	–	–	–	–
$7_0^4 13_0^2$	7.17(7) (s)	–	–	–	–	0.106
?	7.21(1) (w)	–	–	–	–	–
7_0^6	7.25(1) (s,w)	0.144	–	–	–	–
$7_0^5 13_0^2$	7.32(1) (w)	0.144	–	–	–	–
$4p/\pi^*(6b_1)\leftarrow n_{Cl}/\pi(4b_1) + \sigma^*_{CCl}/\sigma^*_{CH}(19a_1)\leftarrow\overline{n}_{Cl}/\sigma_{CC}(16a_1), \left(4^1A_1\leftarrow\widetilde{X}^1A_1\right)$						
0_0^0	7.045	–	–	–	–	–
10_0^1	7.107	–	–	–	0.062	–
10_0^2	7.17(5) (s)	–	–	–	0.068	–
7_0^1	7.188	0.143	–	–	–	–
10_0^3	7.24(0) (w)	–	–	–	0.065	–
7_0^2	7.33(2) (s,w)	0.144	–	–	–	–
7^n	6.98(5) (s)	–	–	–	–	–
7^{n+1}	7.13(0) (s)	0.145	–	–	–	–
7^{n+2}	7.27(4) (w)	0.144	–	–	–	–
	$\overline{\Delta E}$	0.143	0.129	0.069/ 0.072	0.065	0.102

[a] (s) shoulder structure; (w) weak feature; (b) broad structure (the last decimal of the energy value is given in brackets for these less-resolved features); (?) means unassigned feature.

Table 4
Proposed vibrational assignments of 1,2-dichlorobenzene valence and Rydberg series converging to the different ionic states in the photon energy range 7.4 – 9.3 eV[a]. Energies in eV. See text for details.

assignment	energy	ΔE (ν'_7)	ΔE (ν'_8)	ΔE (ν'_9)	ΔE (ν'_{13})
$\pi^*(5b_1)\leftarrow n_{Cl}/\pi(3b_1), \left(6^1A_1\leftarrow\widetilde{X}^1A_1\right)$					
0_0^0	7.61(6) (b)	–	–	–	–
9_0^1	7.68(2) (s,w)	–	–	0.066	–
13_0^1	7.718	–	–	–	0.102
9_0^2	7.74(2) (s,w)	–	–	0.060	–
7_0^1	7.76(4) (s,w)	0.148	0.128	–	–
8_0^1	7.74(4) (s,w)	–	–	–	–
9_0^3	7.800	–	–	0.058	–
$8_0^2/9_0^4$	7.86(5) (s,w)	–	0.121	0.065	–
7_0^2	7.90(7) (s,w)	0.143	–	–	–
7_0^3	8.05(4) (b,w)	0.147	–	–	–
7_0^4	8.192	0.138	–	–	–
$7_0^4 8_0^1/6p(4b_1)^{-1}$	8.31(8) (s)	–	0.126	–	–
7_0^5	8.33(2) (s)	0.140	–	–	–
$7_0^4 8_0^2/8_0^1 6p(4b_1)^{-1}$	8.451	–	0.134	–	–
$7_0^6/5d(4b_1)^{-1}$	8.475	0.143	–	–	–
$7_0^7/7p'(4b_1)^{-1}$	8.62(8) (s)	0.153	–	–	–
7_0^8	8.76(2) (b)	0.134	–	–	–
$5s(4b_1)^{-1}$	7.656	–	–	–	–
9_0^1	7.718	–	–	0.062	–
8_0^1	7.78(1) (s,w)	–	0.125	–	–
7_0^1	7.800	0.144	–	–	–
8_0^2	7.91(0) (s,w)	–	0.129	–	–
7_0^2	7.94(3) (s,w)	0.143	–	–	–
8_0^3	8.03(3) (b)	–	0.123	–	–
8_0^4	8.16(2) (b)	–	0.129	–	–
$4s(14b_2)^{-1}$	7.84(5) (b)	–	–	–	–
$8_0^1/5p'(4b_1)^{-1}$	7.98(4) (s,w)	–	0.139	–	–
$8_0^2/4d(4b_1)^{-1}$	8.12(2) (s,w)	–	0.138	–	–
$8_0^3/6s(4b_1)^{-1}$	8.25(7) (s,w)	–	0.135	–	–
$8_0^4/4s(16a_1)^{-1}$	8.375	–	0.118	–	–
$4s(16a_1)^{-1}$	8.375	–	–	–	–
$8_0^1/4s(3b_1)^{-1}$	8.501	–	0.126	–	–
$8_0^2/7p'(4b_1)^{-1}$	8.62(8) (s)	–	0.127	–	–
$8_0^3/8p'(4b_1)^{-1}$	8.75(0) (s,w)	–	0.122	–	–
$5d/\pi^*(5a_2)\leftarrow n_{Cl}/\pi(4b_1) + \pi^*(5b_1)\leftarrow\overline{n}_{Cl}/\pi(2a_2), \left(6^1B_2\leftarrow\widetilde{X}^1A_1\right)$					
0_0^0	8.09(6) (s,w)	–	–	–	–
9_0^1	8.16(2) (b)	–	–	0.066	–
$8_0^1/9_0^2/4d'(4b_1)^{-1}$	8.222	–	0.126	0.060	–
$9_0^3/8_0^1 9_0^1$	8.288	–	–	0.066	–
$8_0^2/9_0^4$	8.349	–	0.127	0.061	–
$9_0^3 7_0^1/8_0^1 9_0^1 7_0^1$	8.426	0.138	–	–	–

(*continued on next page*)

Table 4 (*continued*)

assignment	energy	ΔE (ν'_7)	ΔE (ν'_8)	ΔE (ν'_9)	ΔE (ν'_{13})
$8_0^3/5d(4b_1)^{-1}$	8.475	–	0.126	–	–
$9_0^3 7_0^2/8_0^1 9_0^1 7_0^2$	8.56(8) (s)	0.142	–	–	–
8^n	8.27(4) (s,w)	–	–	–	–
8^{n+1}	8.52(7) (s)	–	0.126	–	–
8^{n+2}	8.65(8) (w)	–	0.131	–	–
8^{n+3}	8.78(4) (s)	–	0.126	–	–
8^{n+4}	8.91(3) (s)	–	0.129	–	–
$4p(16a_1)^{-1}$	8.54(8) (s,w)	–	–	–	–
7_0^1	8.69(5) (b)	0.147	–	–	–
7_0^2	8.84(0) (b,w)	0.145	–	–	–
$7p(4b_1)^{-1}$	8.58(9) (s)	–	–	–	–
$8_0^1/8s(4b_1)^{-1}$	8.71(6) (s,w)	–	0.127	–	–
$8_0^2/4p'(4b_1)^{-1}/8_0^1 8s(4b_1)^{-1}$	8.84(0) (b,w)	–	0.124	–	–
$6d'(4b_1)^{-1}$	8.69(5) (b)	–	–	–	–
7_0^1	8.83(7) (s,w)	0.142	–	–	–
7_0^2	8.97(1) (s,w)	0.134	–	–	–
7_0^3	9.11(3) (w)	0.142	–	–	–
$9s(4b_1)^{-1}$	8.799	–	–	–	–
$9_0^1/10s(4b_1)^{-1}$	8.862	–	–	0.069	–
$9_0^1 8_0^1/10s(4b_1)^{-1}$	8.98(8) (s,w)	–	0.126	–	–
$9_0^2/11p'(4b_1)^{-1}/9_0^1 10s(4b_1)^{-1}$	8.92(6) (s,w)	–	–	0.058	–
$9_0^1 8_0^2/10s(4b_1)^{-1}$	9.11(3) (w)	–	0.125	–	–
$9p(4b_1)^{-1}$	8.81(8) (s)	–	–	–	–
8_0^1	8.942	–	0.124	–	–
8_0^2	9.07(0) (s,w)	–	0.128	–	–
	$\overline{\Delta E}$	0.143	0.127	0.063	0.102

[a] (b) broad structure; (s) shoulder structure; (w) weak feature (the last decimal of the energy value is given in brackets for these less-resolved features).

5.2. The 5.2–9.3 eV photon energy range

The second absorption band centred at 5.740 eV with a maximum cross-section of 25.59 Mb, is assigned to the valence excitation $\pi^*(4a_2) \leftarrow n_{Cl}/\pi(4b_1) + \pi^*(5b_1) \leftarrow n_{Cl}/\pi(3a_2), \left(1^1B_2 \leftarrow \widetilde{X}^1A_1\right)$ with an oscillator strength $f_L = 0.0405$ (Table 1), which is in good agreement with the EOM-CCSD/aug-cc-pVDZ calculation in Table S2, assigned to the same transition with a value of $f_L = 0.0408$. The 0_0^0 origin band is assigned at 5.53(5) eV (Table 3 and Fig. 3) and shows broad features due to the main vibrational modes ring breathing and C–C stretching, $\nu'_8(a_1)$ and in-plane ring breathing, $\nu'_9(a_1)$ (Table 3) and combination bands of these. Excitation of the asymmetric C–H wagging, $\nu'_{13}(a_2)$, mode would involve two quanta (or even numbers) [38], however single quanta noted may result from coupling with some of the symmetric modes. The lowest-lying $n = 4$ member of the *ns* Rydberg series converging to $(4b_1)^{-1}$ $\widetilde{X}^2B_1$ appears at 5.73(5) eV and contains fine structure assigned to the C–C stretching, $\nu'_8(a_1)$ mode superimposed on the $\left(1^1B_2 \leftarrow \widetilde{X}^1A_1\right)$ transition (see Sec. 5.4). Although the absorption features appear rather broad, which may indicate a more valence character transition of the band, a close inspection of Table S1 shows a transition at ~ 5.985 eV with an oscillator strength $f_L \approx 0.0003$ and assigned to $\sigma^*_{CCl}/\sigma^*_{CH}(19a_1) + 4s/\sigma^*_{CCl}(18a_1) + 4s/\sigma^*_{CCl}(17a_1) \leftarrow n_{Cl}/\pi(4b_1), \left(1^1B_2 \leftarrow \widetilde{X}^1A_1\right)$. This character is in assertion with EOM-CCSD/aug-cc-pVDZ calculation in Table S2, with an electronic excitation at 6.099 eV of mixed valence-Rydberg character with a higher oscillator strength, $f_L = 0.0021$, than in the TD-DFT calculation.

The main absorption band in the VUV spectrum of 1,2-dichlorobenzene peaks at 6.536 eV, with a magnitude of 192.01 Mb (Fig. 1), and is assigned to a valence $\pi^*(4a_2) \leftarrow n_{Cl}/\pi(3a_2) + \pi^*(5b_1) \leftarrow n_{Cl}/\pi(4b_1), \left(3^1A_1 \leftarrow \widetilde{X}^1A_1\right)$ transition in Table 1 with an oscillator strength $f_L =$

Table 5
Proposed vibrational assignments of 1,2-dichlorobenzene valence and Rydberg series converging to the different ionic states in the photon energy range 9.0 – 10.8 eV[a]. Energies in eV. See text for details.

assignment	energy	ΔE (ν'_8)	ΔE (ν'_{10})	ΔE (ν'_{11})
$\{6s/\sigma^*_{CCl}(18a_1) + \sigma^*_{CCl}/\sigma^*_{CH}(19a_1)\} \leftarrow n_{Cl}/\pi(4b_1) + 6d/\sigma^*_{CCl}(19b_2) \leftarrow n_{Cl}/\pi(3a_2), \left(21^1B_1 \leftarrow \widetilde{X}^1A_1\right)$				
$0_0^0/4p(3b_1)^{-1}$	9.20(8)(s)	–	–	–
8_0^1	9.336	0.128	–	–
$8_0^1 10_0^1$	9.39(6)(b)	–	0.060	–
8_0^2	9.46(8)(s,w)	0.132	–	–
$8_0^2 10_0^1$	9.53(7)(s)	0.141	–	–
$8_0^2 10_0^2$	9.58(5)(s)	–	0.048	–
$8_0^3/4p'(16a_1)^{-1}$	9.60(4)(b)	0.136	–	–
$8_0^3 10_0^1$	9.66(7)(s)	–	0.063	–
$8_0^4 10_0^1$	9.80(9)(s)	0.142	–	–
$8_0^5 10_0^1/5p(14b_2)^{-1}$	9.94(1)(b)	0.132	–	–
$\{4d/\pi^*(9b_1) + 4d/\pi^*(10b_1)\} \leftarrow n_{Cl}/\pi(3a_2), \left(16^1B_2 \leftarrow \widetilde{X}^1A_1\right)$				
$8_0^0/5s(14b_2)^{-1}$	9.75(5)(s,w)	–	–	–
10_0^1	9.80(9)(s)	–	0.054	–
8_0^1	9.90(0)(s,w)	0.145	–	–
8_0^2	10.03(3)(w)	0.133	–	–
8_0^3	10.16(6)(b,w)	0.133	–	–
$3d(21a_1) \leftarrow \overline{n}_{Cl}/\sigma_{CC}(16a_1) + \{5s/\sigma^*_{CCl}(18a_1) + \sigma^*_{CCl}/\sigma^*_{CH}(19a_1)\} \leftarrow \sigma_{CCl}/\sigma_{CC}(15a_1), \left(21^1A_1 \leftarrow \widetilde{X}^1A_1\right)$				
0_0^0	10.28(2)(s,w)	–	–	–
11_0^1	10.30(6)(s,w)	–	–	0.024
11_0^2	10.337	–	–	0.031
11_0^3	10.361	–	–	0.024
11_0^4	10.389	–	–	0.028
8_0^1	10.417	0.135	–	–
$11_0^1 8_0^1$	10.442	0.136	–	–
$11_0^1 8_0^1$	10.468	0.131	–	–
$11_0^1 8_0^1$	10.495	0.134	–	–
$11_0^1 8_0^1$	10.521	0.132	–	–
$\pi^*(5b_1) \leftarrow \overline{n}_{Cl}/\pi(2b_1), \left(22^1A_1 \leftarrow \widetilde{X}^1A_1\right)$				
$0_0^0/6p'(14b_2)^{-1}$	10.55(2)(s)	–	–	
11_0^1	10.58(1)(s)	–	–	0.029
$11_0^2/5p(3b_1)^{-1}$	10.604	–	–	0.023
11_0^3	10.626	–	–	0.022
$11_0^4/5d(14b_2)^{-1}/5p'(16a_1)^{-1}$	10.65(2)(b)	–	–	0.026
$8_0^1/5d'(14b_2)^{-1}$	10.67(5)(b)	0.123	–	–
$11_0^1 8_0^1/7s(14b_2)^{-1}$	10.70(3)(b)	0.122	–	–
$11_0^1 8_0^1/7p(14b_2)^{-1}$	10.72(5)(b)	0.118	–	–
$11_0^1 8_0^1$	10.751	0.125	–	–
$11_0^1 8_0^1/7p'(14b_2)^{-1}$	10.77(0)(b)	0.118	–	–
	$\overline{\Delta E}$	0.131	0.051	0.026

[a] (s) shoulder structure; (b) broad structure; (w) weak feature (the last decimal of the energy value is given in brackets for these less-resolved features).

Table 6

Energy values (eV), quantum defects (δ) and assignments of the Rydberg series converging to $(4b_1)^{-1}\ \widetilde{X}^2B_1$, $(14b_2)^{-1}\ \widetilde{B}^2B_2$, $(16a_1)^{-1}\ \widetilde{C}^2A_1$ and $(3b_1)^{-1}\ \widetilde{D}^2B_1$ of 1,2-dichlorobenzene. See text for details.

E_n	δ	assignment	E_n	δ	assignment	E_n	δ	assignment	E_n	δ	assignment
IE$_1$ = 9.075 eV $(4b_1)^{-1}$			**IE$_3$ = 11.236 eV** $(14b_2)^{-1}$			**IE$_4$ = 11.769 eV** $(16a_1)^{-1}$			**IE$_5$ = 11.897 eV** $(3b_1)^{-1}$		
$(ns \leftarrow 4b_1)$			$(ns \leftarrow 14b_2)$			$(ns \leftarrow 16a_1)$			$(ns \leftarrow 3b_1)$		
5.73(5)(b)	1.98	4 s	7.84(5)(b)	2.00	4 s	8.375	2.00	4 s	8.501	2.00	4 s
7.656	1.90	5 s	9.75(5)(s,w)	1.97	5 s	10.25(7)(s,w)	2.00	5 s	10.382	2.00	5 s
8.25(7)(s,w)	1.92	6 s	10.38(6)(b)	2.00	6 s	–	–	–	–	–	–
8.54(8)(s,w)	1.92	7 s	10.70(3)(b)	1.95	7 s	–	–	–	–	–	–
8.71(6)(s,w)	1.84	8 s	–	–	–	–	–	–	–	–	–
8.799	1.98	9 s	–	–	–	–	–	–	–	–	–
8.862	2.00	10 s	–	–	–	–	–	–	–	–	–
$(np \leftarrow 4b_1)$			$(np \leftarrow 14b_2)$			$(np \leftarrow 16a_1)$			$(np \leftarrow 3b_1)$		
6.394	1.75	4p	8.54(8)(s,w)	1.75	4p	9.087	1.75	4p	9.20(8)(s)	1.75	4p
7.78(1)(s,w)	1.76	5p	9.94(1)(b)	1.76	5p	10.491	1.74	5p	10.604	1.76	5p
8.31(8)(s)	1.76	6p	10.46(8)(b)	1.79	6p	–	–	–	–	–	–
8.58(9)(s)	1.71	7p	10.72(5)(b)	1.84	7p	–	–	–	–	–	–
8.72(2)(s)	1.79	8p	–	–	–	–	–	–	–	–	–
8.81(8)(s)	1.72	9p	–	–	–	–	–	–	–	–	–
8.87(8)(w)	1.69	10p	–	–	–	–	–	–	–	–	–
8.92(0)(s,w)	1.63	11p	–	–	–	–	–	–	–	–	–
$(np' \leftarrow 4b_1)$			$(np' \leftarrow 14b_2)$			$(np' \leftarrow 16a_1)$			$(np' \leftarrow 3b_1)$		
–	–	4p'	9.05(3)(s,w)	1.50	4p'	9.60(4)(b)	1.49	4p'	–	–	–
7.98(4)(s,w)	1.47	5p'	10.11(3)(s,w)	1.51	5p'	10.65(2)(b)	1.51	5p'	–	–	–
8.426	1.42	6p'	10.55(2)(s)	1.54	6p'	–	–	–	–	–	–
8.62(8)(s)	1.48	7p'	10.77(0)(b)	1.54	7p'	–	–	–	–	–	–
8.75(0)(s,w)	1.53	8p'	–	–	–	–	–	–	–	–	–
8.84(0)(b,w)	1.39	9p'	–	–	–	–	–	–	–	–	–
8.89(7)(s,w)	1.26	10p'	–	–	–	–	–	–	–	–	–
8.92(6)(s,w)	1.44	11p'	–	–	–	–	–	–	–	–	–
$(nd \leftarrow 4b_1)$			$(nd \leftarrow 14b_2)$			$(nd \leftarrow 16a_1)$			$(nd \leftarrow 3b_1)$		
7.31(5)(b,w)	0.22	3d	9.51(5)(s,w)	0.19	3d	10.00(5)(s)	0.22	3d	10.13(8)(b,w)	0.22	3d
8.12(2)(s,w)	0.22	4d	10.31(1)(s,w)	0.16	4d	–	–	–	–	–	–
8.475	0.24	5d	10.65(2)(b)	0.17	5d	–	–	–	–	–	–
8.67(3)(b,w)	0.18	6d	–	–	–	–	–	–	–	–	–
8.78(4)(s)	0.16	7d	–	–	–	–	–	–	–	–	–
$(nd' \leftarrow 4b_1)$			$(nd' \leftarrow 14b_2)$			$(nd' \leftarrow 16a_1)$			$(nd' \leftarrow 3b_1)$		
–	–	3d'	9.68(6)(b,w)	0.04	3d'	10.21(8)(s,w)	0.04	3d'	10.36(7)(b,w)	0.02	3d'
8.222	0.01	4d'	10.36(7)(b,w)	0.04	4d'	–	–	–	–	–	–
8.52(7)(s)	0.02	5d'	10.67(5)(b)	0.07	5d'	–	–	–	–	–	–
8.69(5)(b)	0.02	6d'	–	–	–	–	–	–	–	–	–
8.799	0.02	7d'	–	–	–	–	–	–	–	–	–
8.862	0.01	8d'	–	–	–	–	–	–	–	–	–

[a](b) broad structure; (s) shoulder structure; (w) weak feature (the last decimal of the energy value is given in brackets for these less-resolved features).

0.6503. The valence character of the electronic transition is in agreement with the EOM-CCSD/aug-cc-pVDZ calculation in Table S2 with a slightly higher oscillator strength (0.7547). A mixed valence-Rydberg character is also expected to contribute to the spectrum. The calculated vertical excitation energy of 6.525 eV (Table 1) is assigned to the $4s/\sigma^*_{CCl}(17a_1) + 4s/\sigma^*_{CCl}(18a_1) \leftarrow n_{Cl}/\pi(4b_1)$, $\left(2^1B_1 \leftarrow \widetilde{X}^1A_1\right)$ transition. However, the quantum defect obtained for the feature in this absorption band suggests the presence of a 4*p* Rydberg series converging to the ionic electronic ground-state, $(4b_1)^{-1}\ \widetilde{X}^2B_1$ (see Sec. 5.4). The next electronic transition peaking at 7.185 eV is assigned in Table 1 to $4p/\pi^*(6b_1) \leftarrow n_{Cl}/\pi(4b_1) + \sigma^*_{CCl}/\sigma^*_{CH}(19a_1) \leftarrow \overline{n}_{Cl}/\sigma_{CC}(16a_1)$, $\left(4^1A_1 \leftarrow \widetilde{X}^1A_1\right)$. Its 0^0_0 origin band is at 7.045 eV and shows a few quanta of the in-plane breathing with C–Cl stretching, $\nu'_7(a_1)$ and the C–Cl symmetric stretching, $\nu'_{10}(a_1)$ modes (Fig. 3 and Table 3). An additional assignment also includes three quanta of $\nu'_7(a_1)$ mode, while its origin was not identifiable, and so the progression has been labelled 7^n.

Above 7.4 eV, the photoabsorption energy range comprises three electronic transitions centred at 7.656, 8.475 and 9.167 eV (Figs. 1, 3 and 4), which are assigned to valence and mixed valence-Rydberg and Rydberg transitions, $\pi^*(5b_1) \leftarrow n_{Cl}/\pi(3b_1)$, $\left(6^1A_1 \leftarrow \widetilde{X}^1A_1\right)$, $5d/\pi^*(5a_2) \leftarrow n_{Cl}/\pi(4b_1) + \pi^*(5b_1) \leftarrow \overline{n}_{Cl}/\pi(2a_2)$, $\left(6^1B_2 \leftarrow \widetilde{X}^1A_1\right)$, $6d/\pi^*(6a_2) \leftarrow n_{Cl}/\pi(4b_1) + \{3d(16b_2) + 4p(15b_2)\} \leftarrow \overline{n}_{Cl}/\sigma_{CC}(16a_1) + \{3d/\sigma^*_{CCl}(20a_1) + \sigma^*_{CCl}/\sigma^*_{CH}(19a_1)\} \leftarrow \overline{n}_{Cl}/\sigma_{CC}(14b_2)$, $\left(10^1B_2 \leftarrow \widetilde{X}^1A_1\right)$, with cross-section values of 21.44, 45.64 and 40.52 Mb, respectively (Table 1). Some of the features have been assigned to Rydberg series converging to $(4b_1)^{-1}\ \widetilde{X}^2B_1$, $(14b_2)^{-1}\ \widetilde{B}^2B_2$, $(16a_1)^{-1}\ \widetilde{C}^2A_1$ and $(3b_1)^{-1}\ \widetilde{D}^2B_1$ ionic states (Table 6). The 0^0_0 origins of these bands are at 7.61(6), 8.09(6) and 9.20 (8) eV, and are mainly accompanied by excitation of in-plane breathing with C–Cl stretching, $\nu'_7(a_1)$, ring breathing and C–C stretching, $\nu'_8(a_1)$, in-plane ring breathing, $\nu'_9(a_1)$, C–Cl symmetric stretching, $\nu'_{10}(a_1)$ and in-plane C–Cl bending $\nu'_{11}(a_1)$ modes, with mean energy values of 0.143, 0.127, 0.063 and 0.057 eV (Tables 4 and 5). Of relevance are the different combination bands involving these modes, and the $\nu'_8(a_1)$ progression appearing at 8.27(4) eV, assigned to 8^n and extending up to 8.91(3) eV, but with no clear evidence of its 0^0_0 origin.

5.3. The 9.3–10.8 eV photon energy range

In this photon energy region (Fig. 5), the absorption features are assigned to valence and mixed valence-Rydberg character accompanied by fine structure (Sec. 5.4). The major electronic transitions $\{6s/\sigma^*_{CCl}(18a_1) + \sigma^*_{CCl}/\sigma^*_{CH}(19a_1)\} \leftarrow n_{Cl}/\pi(4b_1) + 6d/\sigma^*_{CCl}(19b_2) \leftarrow n_{Cl}/\pi(3a_2)$, $\left(21^1B_1 \leftarrow \widetilde{X}^1A_1\right)$ and

$\{4d/\pi^*(9b_1)+4d/\pi^*(10b_1)\}\leftarrow n_{Cl}/\pi(3a_2)$, $\left(16^1B_2\leftarrow\widetilde{X}^1A_1\right)$ have their 0_0^0 origins at 9.20(8) and 9.75(5) eV, and are mainly accompanied by the ring breathing and C–C stretching, $\nu'_8(a_1)$ mode in combination with C–Cl symmetric stretching, $\nu'_{10}(a_1)$, with mean energy values of 0.136 and 0.056 eV (Table 5). Throughout the energy range, the features appear broad, which can be explained in terms of their energy positions being superimposed either on the vibrational progressions or on other Rydberg series contributing to the absorption spectrum. In contrast, above 10.3 eV the spectrum shows fine structure that is somehow better resolved upon a background contribution, suggesting therefore a predissociative character of the electronic transitions. This is in assertion with the character of the higher energy features assigned to valence, mixed-valence Rydberg and Rydberg $3d(21a_1)\leftarrow\bar{n}_{Cl}/\sigma_{CC}(16a_1)+\{5s/\sigma^*_{CCl}(18a_1)+\sigma^*_{CCl}/\sigma^*_{CH}(19a_1)\}\leftarrow\sigma_{CCl}/\sigma_{CC}(15a_1)$, $\left(21^1A_1\leftarrow\widetilde{X}^1A_1\right)$ and $\pi^*(5b_1)\leftarrow\bar{n}_{Cl}/\pi(2b_1)$, $\left(22^1A_1\leftarrow\widetilde{X}^1A_1\right)$ transitions, with oscillator strengths of 0.0553 and 0.0554. Note that in the calculations of Table 1, the dissociative character of the $5s/\sigma^*_{CCl}(18a_1)+\sigma^*_{CCl}/\sigma^*_{CH}(19a_1)\leftarrow\sigma_{CCl}/\sigma_{CC}(15a_1)$, $\left(21^1A_1\leftarrow\widetilde{X}^1A_1\right)$ transition amounts to ≈ 40 %, while across the 9.3–10.8 eV energy range the photoionisation contribution of the $(4b_1)^{-1}$ $\widetilde{X}^2B_1$ ionic state may also render a continuum background to the spectrum. The 0_0^0 origins are tentatively suggested at 10.28(2) and 10.55(2) eV (Table 5 and Fig. 5) however we are not able to provide their vertical excitation energies and local maximum cross-section values (Table 1).

5.4. Rydberg transitions

The photoabsorption features that are tentatively assigned to Rydberg transitions converging to the different ionic states of 1,2-dichlorobenzene are listed in Table 6 together with their quantum defects. The features' positions have been tested using the Rydberg formula, $E_n = IE - \frac{R}{(n-\delta)^2}$, where IE is the ionisation energy of a given MO, n is the principal quantum number of the Rydberg orbital of energy E_n, R is the Rydberg constant (13.61 eV), and δ is the quantum defect resulting from the penetration of the Rydberg orbital into the core.

The Rydberg character of the absorption features is prominently observed above 5.2 eV, with fine structure superimposed on it. In polyatomic molecules as 1,2-dichlorobenzene is, the photoabsorption spectrum shows most of the vibronic transitions rather enhanced, typically above the lowest-lying members of the Rydberg series. A thorough literature survey shows no previous Rydberg assignments, and so the fine structure discernible on the different Rydberg transitions up to 10.8 eV, are listed in Tables 3–5. Note that in Tables 4 and 5, some of the proposed assignments obtained from the quantum defects estimate, are not supported by the calculations on the Rydberg states.

The lowest-lying Rydberg transition ($n = 4$) converging to the ionic electronic ground-state IE$_1$, $(4b_1)^{-1}$, is assigned to the $(4s\leftarrow 4b_1)$ excitation, with the first member at 5.73(5) eV and having a quantum defect $\delta = 1.98$. Other higher-order Rydberg members of the *ns* series, up to the $n = 10$, are also reported in Table 6. The first member of the n*p* $(np\leftarrow 4b_1)$ series has an absorption feature at 6.394 eV ($\delta = 1.75$) whereas for the $(np'\leftarrow 4b_1)$ series we were not able to obtain any discernible feature in the absorption spectrum. Table 6 also includes two n*d* $(nd\leftarrow 6a'')$ and $(nd'\leftarrow 6a'')$ series, where only $n = 3d$ is visible at 7.31(5) eV ($\delta = 0.22$). Other transitions to the *nd* and *nd'* Rydberg members, up to $n = 7$ and 8, are also visible. The features at 8.54(8), 8.799 and 8.862 eV can also be assigned to $4p(14b_2)^{-1}$, $7d'(4b_1)^{-1}$ and $8d'(4b_1)^{-1}$, respectively.

The Rydberg series converging to the ionic electronic second excited state IE$_3$, $(14b_2)^{-1}$, are listed in Table 6, and have been assigned to the $(ns, np, np', nd, nd'\leftarrow 14b_2)$ transitions. The first members of these series (either $n = 4$ or $n = 3$) are associated with features at 7.84(5) eV ($\delta = 2.00$), 8.54(8) eV ($\delta = 1.75$), 9.05(3) eV ($\delta = 1.50$), 9.51(5) eV ($\delta = 0.19$) and 9.68(6) eV ($\delta = 0.04$) (Table 6). The features at 10.65(2) and 10.36 (7) eV can also be assigned to $5p'(16a_1)^{-1}$ and $3d'(3b_1)^{-1}$.

The Rydberg series converging to the ionic electronic third excited state IE$_4$, $(16a_1)^{-1}$, have been assigned to the $(ns, np, np', nd, nd'\leftarrow 16a_1)$ transitions. The first members of these series (either $n = 4$ or $n = 3$) have features at 8.375 eV ($\delta = 2.00$), 9.087 eV ($\delta = 1.75$), 9.60(4) eV ($\delta = 1.49$), 10.00(5) eV ($\delta = 0.22$) and 10.36(7) eV ($\delta = 0.02$) (Table 6).

The Rydberg series converging to IE$_5$, $(3b_1)^{-1}$, has been assigned to the $(ns, np, nd, nd'\leftarrow 3b_1)$ transitions. These show only a few members up to $n = 5$ for the *ns* and *np* series with only n = 3 for *nd* (Table 6). Assignments for higher members have not been performed because they lie outside the photon energy range investigated.

As noted before, the absorption spectrum contains different members of Rydberg transitions accompanied by fine structure resulting from the different vibronic transitions, which have been assigned in Tables 3–5. The information on the modes contributing to the spectrum has been obtained from the main vibrational modes in the experimental photoelectron spectrum of Holland *et al.* [19]. These are from the in-plane breathing with C–Cl stretching, $\nu'_7(a_1)$, ring breathing and C–C stretching, $\nu'_8(a_1)$, in-plane ring breathing, $\nu'_9(a_1)$, C–Cl symmetric stretching, $\nu'_{10}(a_1)$ and in-plane C–Cl bending $\nu'_{11}(a_1)$ modes, together with combination. Also, only two quanta of the asymmetric C–H wagging, $\nu'_{13}(a_2)$, mode have been assigned for the lowest-lying Rydberg member $4p(4b_1)^{-1}$.

5.5. Potential energy curves along the C–Cl bending and C–Cl stretching coordinates

We have performed calculations at the TD-DFT/CAMB3LYP/aug-cc-pVDZ level of theory in the C_1 symmetry group of the potential energy curves (PECs) along the C–Cl stretching and C–Cl in-plane bending coordinates, $\nu'_{10}(a_1)$ and $\nu'_{11}(a_1)$, while allowing all the other geometric parameters to relax following the respective mode. The results for the ten lowest-lying singlet excited states of 1,2-dichlorobenzene are shown in Fig. 6.

Fig. 6 a) shows that all states have bound characters along the C–Cl symmetric stretching coordinate. The first excited singlet–singlet electronic transition in the photoabsorption spectrum of Fig. 2 assigned to $\pi^*(5b_1)\leftarrow n_{Cl}/\pi(4b_1)+\pi^*(4a_2)\leftarrow n_{Cl}/\pi(3a_2)$, $\left(2^1A_1\leftarrow\widetilde{X}^1A_1\right)$, shows several quanta of C–Cl symmetric stretching, $\nu'_{10}(a_1)$ mode in the photon energy range 4.2 − 5.3 eV (see also Table 2). A close inspection of the PECs shows some avoided crossings which are more noticeable for the four lowest-lying excited states between 0.3 a_0 and 1.0 a_0. Within the nuclear dynamics description of an adiabatic behaviour at these avoided crossings, the electronic nature of the initially accessible MO may change its character as the vibrational modes within the molecular frame are allowed to relax. We have comprehensively checked the character of some of the electronic transitions from the ground-state to each excited-state at different interatomic displacements to infer internal conversion mechanisms. These results are plotted in Fig. S6 (see e.g. for second and third excited states) and show the change from valence (π*) to Rydberg character as one moves from shortening to stretching the bond. At higher energies, the potential-wells tend to be shallower which may result in a more dissociative character. Additionally, these states appear almost degenerate at R_{C-Cl} equilibrium distance (e.g. 4th to 7th), because they originate from the same MOs, i.e., either the HOMO (n_{Cl}/π, $4b_1$) or the HOMO-1 (n_{Cl}/π, $3a_2$). Together with the remaining states at energies > 7.0 eV, they all cross slightly above the equilibrium internuclear distance. This may render an important adiabatic character, which can be responsible for Rydberg to valence internal conversion in the asymptotic limit where C–Cl bond excision may be a prevalent mechanism.

Turning to the PECs in Fig. 6 b), along the in-plane C–Cl bending $\nu'_{11}(a_1)$ mode. A close comparison with Fig. 6 a) shows similarities for

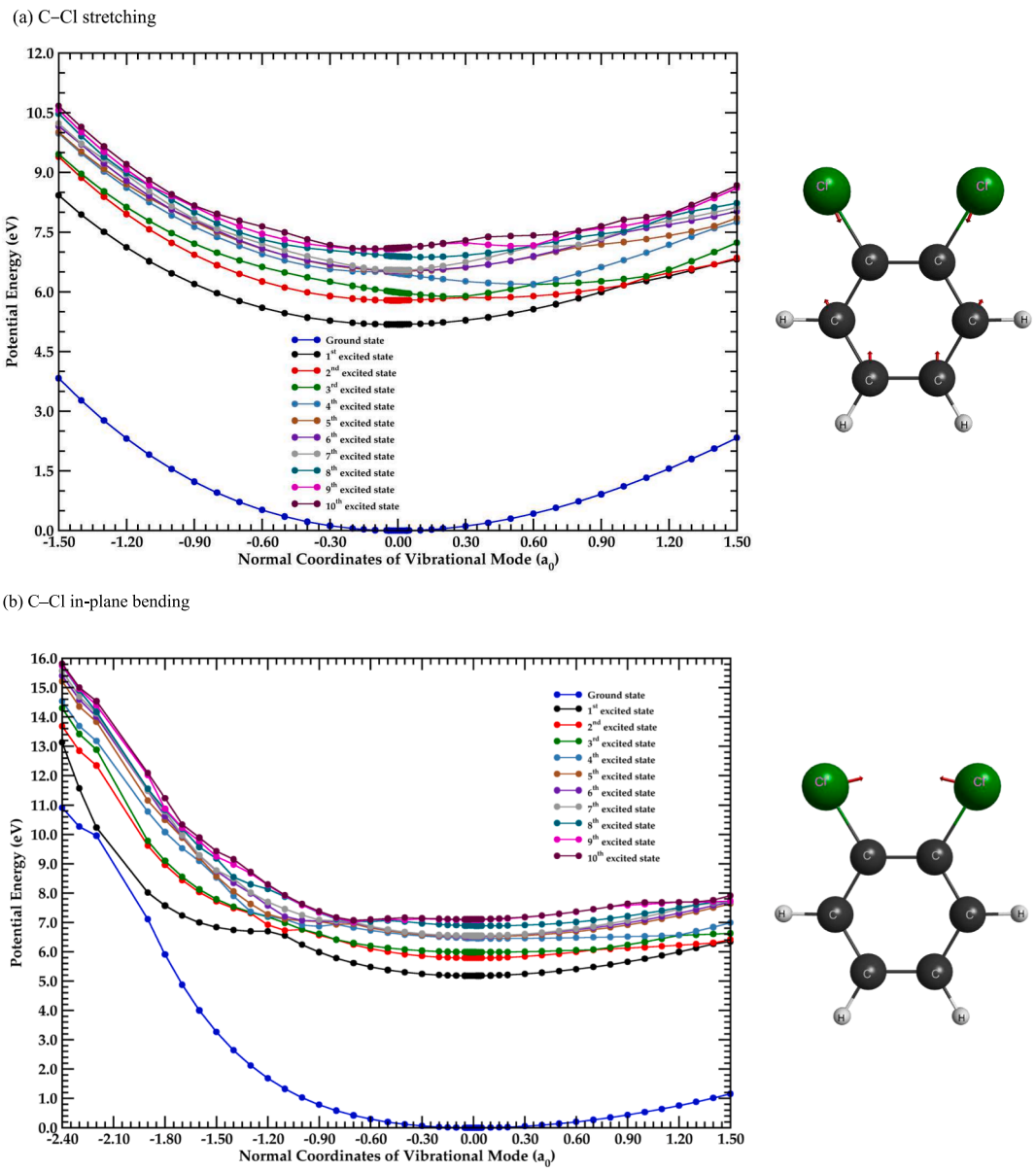

Fig. 6. PECs for the ten lowest-lying excited singlet states of the 1,2-dichlorobenzene plotted following the C–Cl stretching and C–Cl in-plane bending modes, $\nu'_{10}(a_1)$ and $\nu'_{11}(a_1)$ (in a_0 units), while allowing all vibrational modes to relax. The calculations were performed at the TD-DFT/CAMB3LYP/aug-cc-pVDZ level of theory in the C_1 symmetry group. See text for details.

the normal coordinates' positive values, whilst significant differences are noted as the two chlorine atoms are brought together (negative normal coordinated). In the lowest-lying excited state as one bends the C–Cl bonds below the internuclear distance, and as the ~ 2 eV barrier height (at −1.20 a_0) is surpassed, the two chlorine atoms can yield Cl_2. This is in good agreement with the time-of-flight mass spectrometry data of Kumar *et al.* [25] on the geometrical effect of chlorine atom positions in C_6Cl_6 and 1,2-dichlorobenzene molecules yielding Cl_2^-. In this study such anion formation is obtained after capturing a low-energy electron, with the two closest C–Cl bonds being cleaved while the chlorine atoms are brought together. Moreover, Kumar et al. [25] have also shown with quantum thermochemical extrapolation methods G4MP2 [39,40] and CBS-QB3 [41,42], that in the neutral molecules, Cl_2 can also be formed through transition states with a barrier height estimated in < 2.0 eV. For further details see ref. [25].

The lowest-lying excited PEC is quasi-degenerate with the second excited state and as the normal coordinate mode moves apart, i.e. towards positive values, this state can reach with almost no energy expense states that are dissociative in their asymptotic limits close to + 1.2 a_0 where internal conversion from valence to Rydberg and vice-versa (Fig. S7) may occur.

5.6. *Absolute photoabsorption cross sections and atmospheric photolysis*

The present absolute ultraviolet photoabsorption cross-sections of 1,2-dichlorobenzene are reported in the photon energy region 4.0–10.8 eV, with Table 1 listing the major electronic transitions and their values in units of Mb. Previous study of the vacuum ultraviolet photoabsorption has covered the wavelength region 43 000 to 60 000 cm^{-1} (5.331 to 7.439 eV) [17], and are found to be in reasonable agreement with the present cross-sections in shape and magnitude. Scharping and Zetzsch [17] report at 6.5 eV a cross-section value of ~ 210 Mb which is ~ 9 % higher than our value of 192.01 Mb. The other experimental value at ~ 5.75 eV with magnitude ≈ 28 Mb also compares quite well with our corresponding result of 25.59 Mb.

Photolysis rates of 1,2-dichlorobenzene in the Earth's atmosphere,

from 0 km (sea-level) up to an altitude of 50 km (the limit of the stratopause), have been calculated from the combination of the present high-resolution VUV absolute photoabsorption cross-sections and the NASA solar actinic flux measurements [43]. This procedure has been used on several occasions before, with details being found from the work of Limão-Vieira *et al.* [44]. The quantum yield for dissociation is assumed to be 1.0, since a literature survey has revealed no reference to such value from photodissociation studies. Photolysis lifetimes of less than 1 sunlit days were calculated at altitudes above 21 km suggesting that UV photolysis can be a relevant removal mechanism of any 1,2-dichlorobenzene in the stratosphere. However, at lower altitudes (< 20 km) the photolysis lifetimes can reach several sunlit days, meaning that this molecule cannot be efficiently broken up by UV radiation. Moreover, from the photodissociation of 1,2-dichlorobenzene at 266 nm (4.661 eV) yielding $C_6H_4Cl^{\bullet}$ and $Cl^{\bullet}$, the photofragment translational energy distribution together with the angular distribution of photofragments, estimate that 23 % of the available energy is assigned to translational energy, thus suggesting that *o*-$C_6H_4Cl_2$ photodissociation is a slow process [45].

Masten and co-workers [13] have investigated the gas-phase reaction of 1,2-dichlorobenzene with the •OH radical, having obtained a rate value of $k_{OH} = 6.64 \times 10^{-18}$ dm^3 $molecule^{-1}$ s^{-1}. The authors reported this reaction to be mainly responsible for the degradation process of this molecule. However, we are neither aware of another work in the literature assessing this reaction as the main sink mechanism in the Earth's atmosphere nor the role of other reactional processes that may prevail.

6. Conclusions

The present joint experimental and theoretical investigation of 1,2-dichlorobenzeze electronic state spectroscopy provides the most comprehensive study to date of this molecule in the energy range 4.0–10.8 eV (310–115 nm). The high-resolution absolute photoabsorption spectrum shows features have been assigned to valence, mixed valence-Rydberg and Rydberg transitions with the aid of quantum chemical calculations, on the vertical excitation energies and oscillator strengths at two different levels of theory. The detailed analysis of the absorption structures in the photoabsorption spectrum has also allowed us to propose assignments for the in-plane breathing with C–Cl stretching, $\nu'_7(a_1)$, ring breathing and C–C stretching, $\nu'_8(a_1)$, in-plane ring breathing, $\nu'_9(a_1)$, C–Cl symmetric stretching, $\nu'_{10}(a_1)$ and in-plane C–Cl bending $\nu'_{11}(a_1)$ modes.

The photolysis lifetimes of 1,2-dichlorobenzene were also obtained for the Earth's atmosphere, from 0 km up to 50 km altitude, which indicate that solar photolysis is not expected to be a sink mechanism at altitudes lower than 20 km. Finally, potential energy curves as a function of the C–Cl stretching and C–Cl in-plane bending coordinates, for the lowest-lying excited states, were calculated at the TD-DFT/CAMB3LYP/aug-cc-pVDZ level of theory. The normal mode description within the framework of the complex nuclear dynamics shows the importance of the close lying excited states as the reaction coordinates are changed from their equilibrium distances, with relevant avoided crossings responsible for internal conversion processes from initial Rydberg states to final valence character and/or vice-versa.

CRediT authorship contribution statement

L.V.S. Dalagnol: Software, Formal analysis, Data curation. **S. Kumar:** Investigation. **A.Souza Barbosa:** Data curation, Investigation, Methodology, Software, Writing – review & editing. **U.S. Akther:** Visualization, Resources, Methodology, Data curation. **N.C. Jones:** Writing – review & editing, Writing – original draft, Visualization, Validation, Supervision, Resources, Methodology, Investigation. **S.V. Hoffmann:** Writing – review & editing, Writing – original draft, Supervision, Resources, Project administration, Methodology, Investigation, Funding acquisition, Conceptualization. **M.H.F. Bettega:** Writing – review & editing, Writing – original draft, Software, Resources, Funding acquisition, Formal analysis, Data curation, Conceptualization. **P. Limão-Vieira:** Conceptualization, Data curation, Formal analysis, Funding acquisition, Investigation, Project administration, Supervision, Validation, Writing – original draft, Writing – review & editing.

Declaration of competing interest

The authors declare that they have no known competing financial interests or personal relationships that could have appeared to influence the work reported in this paper.

Acknowledgments

MHFB acknowledges the Brazilian agency Coordenação de Aperfeiçoamento de Pessoal de Nível Superior (CAPES) and together with LVSD and ASB the support from the Brazilian agency Conselho Nacional de Desenvolvimento Científico e Tecnológico (CNPq). LVSD, ASB and MHFB also acknowledge Prof. Carlos A. M. de Carvalho for computational support at LFTC-DFis-UFPR and at LCPAD-UFPR. The authors wish to acknowledge the beam time at the ISA synchrotron, Aarhus University, Denmark. The research leading to this result has been supported by the project CALIPSOplus under the Grant Agreement 730872 from the EU Framework Programme for Research and Innovation HORIZON 2020. PLV acknowledges the Portuguese National Funding Agency (FCT) through research grant CEFITEC (UIDB/00068/2020), his visiting professor position at Federal University of Paraná, Curitiba, Brazil and the support from CAPES PrInt/UFPR. This work was also supported by Radiation Biology and Biophysics Doctoral Training Programme (RaBBiT, PD/00193/2012) and UCIBIO (UIDB/04378/2020).

Appendix A. Supplementary data

Supplementary data to this article can be found online at https://doi.org/10.1016/j.jphotochem.2024.116153.

Data availability

Data will be made available on request.

References

[1] D. Duflot, S.V. Hoffmann, N.C. Jones, P. Limão-Vieira, Synchrotron radiation UV-VUV photoabsorption of gas phase molecules, in: A.S. Pereira, P. Tavares, P. Limão-Vieira (Eds.), Radiat, Springer, Bioanal. Spectrosc. Tech. Theor. Methods, 2019, pp. 43–81.

[2] P.A.S. Randi, D.F. Pastega, M.H.F. Bettega, N.C. Jones, S.V. Hoffmann, S. Eden, A. S. Barbosa, P. Limão-Vieira, Electronically excited states of formic acid investigated by theoretical and experimental methods, Spectrochim, Acta, Part a. 289 (2023) 122237, https://doi.org/10.1016/j.saa.2022.122237.

[3] F.V.S. Oliveira, A.S. Barbosa, N.C. Jones, S.V. Hoffmann, P. Limão-Vieira, The electronic spectra of 2- chlorothiophene and 3-chlorothiophene in the vacuum ultraviolet photoabsorption energy region (3.9–10.8 eV), J. Quant. Spectrosc. Radiat. Transf. 296 (2023) 108443, https://doi.org/10.1016/j.jqsrt.2022.108443.

[4] E. Lange, N.C. Jones, S.V. Hoffmann, A.I. Lozano, S. Kumar, M.G.P. Homem, M. A. Śmiałek, D. Duflot, M.J. Brunger, P. Limão-Vieira, The electronic excited states of dichloromethane in the 5.8-10.8 eV energy range investigated by experimental and theoretical methods, J. Quant. Spectrosc. Radiat. Transf. 253 (2020) 107172, https://doi.org/10.1016/j.jqsrt.2020.107172.

[5] L.V.S. Dalagnol, M.H.F. Bettega, N.C. Jones, S.V. Hoffmann, A.S. Barbosa, P. Limão-Vieira, Electronic State Spectroscopy of Nitromethane and Nitroethane, J. Phys. Chem. a. 127 (2023) 1445–1457, https://doi.org/10.1021/acs.jpca.2c08023.

[6] A.S. Barbosa, M. Mendes, N.C. Jones, S.V. Hoffmann, M.H.F. Bettega, M.J. Brunger, P. Limão-Vieira, Low-lying electronic states of ethanol investigated by theoretical and synchrotron radiation methods, J. Quant. Spectrosc. Radiat. Transf. 285 (2022) 108170, https://doi.org/10.1016/j.jqsrt.2022.108170.

[7] M. Mendes, K. Regeta, F.F. Silva, N.C. Jones, S.V. Hoffmann, G. García, C. Daniel, P. Limão-Vieira, Comprehensive investigation of the electronic excitation of W(CO) 6 by photoabsorption and theoretical analysis in the energy region from 3.9 to 10.8

eV, Beilstein J. Nanotechnol. 8 (2017) 2208–2218, https://doi.org/10.3762/bjnano.8.220.
[8] P.A.S. Randi, G.M. Moreira, M.H.F. Bettega, Electron collisions with formic acid, Eur. Phys. J. d. 75 (2021) 306.
[9] P.A.S. Randi S. Kumar A.S. Barbosa U.S. Akther N.C. Jones S.V. Hoffmann M.H.F. Bettega P. Limão-Vieira The electronic states of 2-chlorotoulene in the 4.0-10.8 eV photon energy rangetle Spectrochim. Acta, Part a. 2024 submitted.
[10] I. Martí, R. Lloret, J. Martín-Alonso, F. Ventura, Determination of chlorinated toluenes in raw and treated water samples from the Llobregat river by closed loop stripping analysis and gas chromatography-mass spectrometry detection, J. Chromatogr. a. 1077 (2005) 68–73, https://doi.org/10.1016/j.chroma.2005.04.051.
[11] D. Dobslaw, K.H. Engesser, Biodegradation of gaseous emissions of 2-chlorotoluene by strains of Rhodococcus sp. in polyurethane foam packed biotrickling filters, Sci. Total Environ. 639 (2018) 1491–1500, https://doi.org/10.1016/j.scitotenv.2018.05.278.
[12] L. Li, D. Zhang, W. Hu, Y. Yang, S. Zhang, R. Yuan, P. Lv, W. Zhang, Y. Zhang, Y. Zhang, Improving VOC control strategies in industrial parks based on emission behavior, environmental effects, and health risks: A case study through atmospheric measurement and emission inventory, Sci. Total Environ. 865 (2023) 161235, https://doi.org/10.1016/j.scitotenv.2022.161235.
[13] S.J. Masten, M. Shu, M.J. Galbraith, S.H.R. Davies, Oxidation of chorinated benzenes using advanced oxidation processes, Hazard. Was. Hazard. Mater. 13 (1996) 265–282, https://doi.org/10.1080/01919512.1997.10382862.
[14] C. Xie, T. Heumüller, W. Gruber, X. Tang, A. Classen, I. Schuldes, M. Bidwell, A. Späth, R.H. Fink, T. Unruh, I. McCulloch, N. Li, C.J. Brabec, Overcoming efficiency and stability limits in water-processing nanoparticular organic photovoltaics by minimizing microstructure defects, Nat. Commun. 9 (2018) 5335, https://doi.org/10.1038/s41467-018-07807-5.
[15] Z. Ma, B. Zhao, Y. Gong, J. Deng, Z. Tan, Green-solvent-processable strategies for achieving large-scale manufacture of organic photovoltaics, J. Mater. Chem. a. 7 (2019) 22826–22847, https://doi.org/10.1039/c9ta09277c.
[16] A. Gaber, M. Riese, J. Grotemeyer, Mass analyzed threshold ionization spectroscopy of o-, m-, and p-dichlorobenzenes. Influence of the chlorine position on vibrational spectra and ionization energy, J. Phys. Chem. a. 112 (2008) 425–434, https://doi.org/10.1021/jp074802t.
[17] H. Scharping, C. Zetzsch, Substituent effects in the VUV absorption spectra of monochlorobenzene and o-, m-, and p-dichlorobenzene, J. Mol. Spectrosc. 112 (1985) 8–17, https://doi.org/10.1016/0022-2852(85)90186-9.
[18] J.H.S. Green, Vilbrational spectra of benzene derivatives-IX . o-Disubstituted compounds, Spectrochim. Acta. 26A (1970) 1913–1923.
[19] D.M.P. Holland, I. Powis, A.B. Trofimov, I.L. Bodzuk, D.Y. Soshnikov, A.W. Potts, L. Karlsson, A study of the valence shell electronic structure and photoionisation dynamics of ortho-dichlorobenzene, ortho-bromochlorobenzene and trichlorobenzene, Chem. Phys. 448 (2015) 61–75, https://doi.org/10.1016/j.chemphys.2014.11.025.
[20] J.P. Maier, O. Marthaler, Emission Spectra of the Radical Cations of 1,3-dichlorobenzene, 1,4-complex multidimensional character of the potential energy surfaces involved and 1,3,5-trichlorobenzene in the Gas Phase, Chem. Phys. 32 (1978) 419–427.
[21] B. Ruščić, L. Klasinc, A. Wolf, J.V. Knop, Photoelectron spectra of and ab initio calculations on chlorobenzenes. 2. Trichlorobenzenes, tetrachlorobenzenes, and pentachlorobenzene, J. Phys. Chem. 85 (1981) 1486–1489, https://doi.org/10.1021/j150611a008.
[22] K. Watanabe, Ionization potentials of some molecules, J. Quant. Spectrosc. Radiat. Transf. 2 (1957) 369–382, https://doi.org/10.1063/1.1743340.
[23] S. Fujisawa, I. Oonishi, S. Masuda, K. Ohno, Y. Harada, Penning ionization electron spectroscopy of nitriles, J. Phys. Chem. 95 (1991) 4250–4254, https://doi.org/10.1021/j150646a010.
[24] S.G. Lias, P. Ausloos, Ionization Energies of Organic Compounds by Equilibrium Measurements, J. Am. Chem. Soc. 100 (1978) 6027–6034, https://doi.org/10.1021/ja00487a009.
[25] S. Kumar, J. Romero, M. Probst, T. Maihom, G. García, P. Limão-Vieira, Sensing the ortho Positions in C6Cl6 and C6H4Cl2 from Cl2− Formation upon Molecular Reduction, Molecules 27 (2022) 4820, https://doi.org/10.3390/molecules27154820.
[26] S. Eden, P. Limão-Vieira, S.V. Hoffmann, N.J. Mason, VUV photoabsorption in CF3X (X = Cl, Br, I) fluoro-alkanes, Chem. Phys. 323 (2006) 313–333.
[27] M.H. Palmer, T. Ridley, S.V. Hoffmann, N.C. Jones, M. Coreno, M. De Simone, C. Grazioli, M. Biczysko, A. Baiardi, P. Limão-Vieira, Interpretation of the vacuum ultraviolet photoabsorption spectrum of iodobenzene by ab initio computations, J. Chem. Phys. 142 (2015) 134302.
[28] R. Bauernschmitt, R. Ahlrichs, Treatment of electronic excitations within the adiabatic approximation of time dependent density functional theory, Chem. Phys. Lett. 256 (1996) 454–464.
[29] M.E. Casida, Time-dependent density-functional theory for molecules and molecular solids, J. Mol. Struct.-Theochem. 914 (2009) 3–18.
[30] T. Yanai, D.P. Tew, N.C. Handy, A new hybrid exchange-correlation functional using the Coulomb-attenuating method (CAM-B3LYP), Chem. Phys. Lett. 393 (2004) 51–57.
[31] R.A. Kendall, T.H. Dunning, R.J. Harrison, Electron affinities of the first-row atoms revisited. Systematic basis sets and wave functions, J. Chem. Phys. 96 (1992) 6796–6806, https://doi.org/10.1063/1.462569.
[32] G.M.J. Barca, C. Bertoni, L. Carrington, D. Datta, N. De Silva, J.E. Deustua, D. G. Fedorov, J.R. Gour, A.O. Gunina, E. Guidez, T. Harville, S. Irle, J. Ivanic, K. Kowalski, S.S. Leang, H. Li, W. Li, J.J. Lutz, I. Magoulas, J. Mato, V. Mironov, H. Nakata, B.Q. Pham, P. Piecuch, D. Poole, S.R. Pruitt, A.P. Rendell, L.B. Roskop, K. Ruedenberg, T. Sattasathuchana, M.W. Schmidt, J. Shen, L. Slipchenko, M. Sosonkina, V. Sundriyal, A. Tiwari, J.L. Galvez Vallejo, B. Westheimer, M. Włoch, P. Xu, F. Zahariev, M.S. Gordon, Recent developments in the general atomic and molecular electronic structure system, J. Chem. Phys. 152 (2020) 154102.
[33] K. Emrich, An extension of the coupled cluster formalism to excited states (I), Nucl. Phys. A 351 (1981) 379–396.
[34] H. Sekino, R.J. Bartlett, A linear response, coupled-cluster theory for excitation energy, Int. J. Quantum Chem. 26 (1984) 255–265.
[35] J.F. Stanton, R.J. Bartlett, The equation of motion coupled-cluster method. A systematic biorthogonal approach to molecular excitation energies, transition probabilities, and excited state properties, J. Chem. Phys. 98 (1993) 7029–7039.
[36] R.J. Bartlett, Coupled-cluster theory and its equation-of-motion extensions, Wiley Interdiscip. Rev. Comput. Mol. Sci. 2 (2012) 126–138.
[37] A. Gaber, M. Riese, J. Grotemeyer, Detailed analysis of the cation ground state of three dichlorobenzenes by mass analyzed threshold ionization spectroscopy, Phys. Chem. Chem. Phys. 10 (2008) 1168–1176, https://doi.org/10.1039/b715496h.
[38] G. Herzberg, Molecular Spectra and Molecular Structure, Vol. III, Van Nostrand, New Jersey, 1967.
[39] L.A. Curtiss, P.C. Redfern, K. Raghavachari, Gaussian-4 theory, J. Chem. Phys. 126 (2007) 084108, https://doi.org/10.1063/1.2436888.
[40] L.A. Curtiss, P.C. Redfern, K. Raghavachari, Gaussian-4 theory using reduced order perturbation theory, J. Chem. Phys. 127 (2007) 124105, https://doi.org/10.1063/1.2770701.
[41] J.A. Montgomery, M.J. Frisch, J.W. Ochterski, G.A. Petersson, A complete basis set model chemistry. VI. Use of density functional geometries and frequencies, J. Chem. Phys. 110 (1999) 2822–2827, https://doi.org/10.1063/1.477924.
[42] J.A. Montgomery, M.J. Frisch, J.W. Ochterski, G.A. Petersson, A complete basis set model chemistry. VII. Use of the minimum population localization method, J. Chem. Phys. 112 (2000) 6532–6542, https://doi.org/10.1063/1.481224.
[43] Chemical Kinetics and Photochemical Data for Use in Stratospheric Modelling, Evaluation number 12, NASA, Jet Propulsion Laboratory, JPL, Publication 97-4, January 15, 1997.
[44] P. Limão-Vieira, S. Eden, P.A. Kendall, N.J. Mason, S.V. Hoffmann, VUV photoabsorption cross-section for CCl2F2, Chem. Phys. Lett. 364 (2002), https://doi.org/10.1016/S0009-2614(02)01304-0.
[45] R.-S. Zhu, H. Zhang, G.-J. Wang, X.-B. Gu, K.-L. Han, G.-Z. He, N.-Q. Lou, Photodissociation of o-dichlorobenzene at 266 nm, Chem. Phys. 287 (2003) 285–294, https://doi.org/10.1016/S0301-0104(02)01007-8.